arXiv:2110.12734v3 [cs.CV] 4 Feb 2022

Fast Gradient Non-sign Methods

Yaya Cheng, Jingkuan Song, Xiaosu Zhu, Qilong Zhang, Lianli Gao, Heng Tao Shen *Fellow, IEEE*

***Abstract*—Adversarial attacks make their success in "fooling" DNNs, and among them, gradient-based algorithms become one of the mainstreams. Based on the linearity hypothesis [1], under ℓ_∞ constraint, $sign$ operation applied to the gradients is a good choice for generating perturbations. However, side-effects from such operation exist since it leads to the bias of direction between real gradients and perturbations. In other words, current methods contain a gap between real gradients and actual noises, which leads to biased and inefficient attacks. Therefore in this paper, based on the Taylor expansion, the bias is analyzed theoretically, and the correction of sign, *i.e.*, Fast Gradient Non-sign Method (FGNM), is further proposed. Notably, FGNM is a general routine that seamlessly replaces the conventional $sign$ operation in gradient-based attacks with negligible extra computational cost. Extensive experiments demonstrate the effectiveness of our methods. Specifically, for untargeted black-box attacks, ours outperform them by 27.5% at most and 9.5% on average. For targeted attacks against defense models, it is 15.1% and 12.7%. Our anonymous code is publicly available: https://github.com/yaya-cheng/FGNM.**

***Index Terms*—Image Classification, Adversarial Attack, Gradient-based Methods.**

I. Introduction

RESEARCHERS have noticed that, by applying human-imperceptible perturbations, some "special" inputs will lead DNNs to give unreasonable outputs, which facilitates the born of adversarial attacks [1]–[11]. Although a series of DNNs have shown their incredible performance in computer vision tasks, their vulnerability is still a severe problem as their explosive development in recent years [12]–[18]. It is vital to learn to generate adversarial examples since it can help to evaluate and improve robustness of DNNs.

Several methods have been proposed to craft adversarial examples. In general, adversarial attacks can be grouped into two categories: non-targeted attacks and targeted attacks. For targeted attacks, adversaries should induce victim's models to output specific wrong label. For non-targeted attacks, adversarial example is expected to mislead victim's models to output an arbitrary class except the original one. As a popular branch both in targeted and non-targeted attacks, gradient-based methods focus on how to produce proper perturbations based on gradients, such as one-step attacks [1], [5] and iterative-step attacks [2]–[4]. By taking the ascending direction of gradient of an objective function $\mathcal{L}$, *e.g.*, cross-entropy, perturbations are obtained and adversarial examples are pulled away from the original decision boundary. To make adversarial examples further away from this decision boundary and reduce computational overhead, most gradient-based methods decide to craft adversarial examples by performing sign operations according to the linearity hypothesis [1]. In particular, given a linear model $\mathcal{F}(\boldsymbol{x}) = \boldsymbol{w}^\mathsf{T}\boldsymbol{x} + \boldsymbol{b}$, adversarial perturbations $\boldsymbol{\eta}$ can increase activation value and this growth is linearly related to weight vector $\boldsymbol{w}$. Satisfying the max norm constraint on adversarial perturbations, Goodfellow *et al*. maximize the activation change by assigning $\boldsymbol{\eta} = \mathrm{sign}(\boldsymbol{w})$.

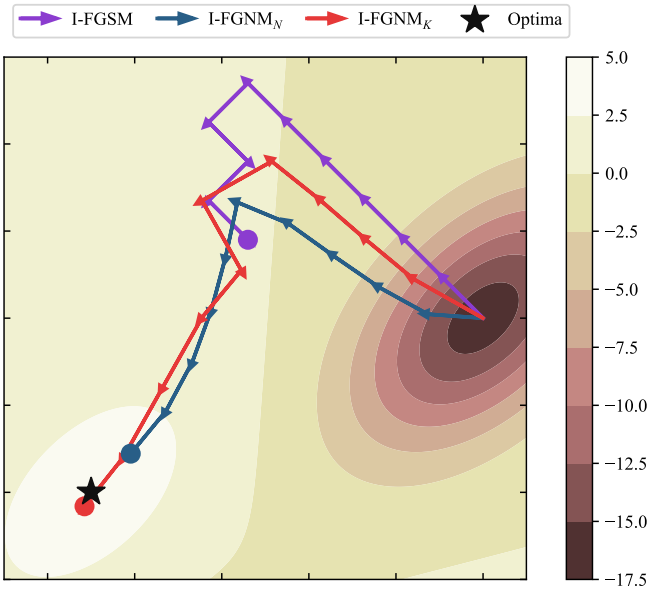


Fig. 1: Visualization on a toy example of climbing mountain with traditional I-FGSM and our I-FGNM variants. Specifically, when adopting I-FGSM, the trajectory is biased due to the limitation of sign. It can not approach the optima and results in oscillation. Our I-FGNM$_\mathrm{N}$ holds the identical step size with I-FGSM in each iteration, but produces a more precise trajectory and is close to the optima. The I-FGNM$_\mathrm{K}$ considers the trade-off between magnitude and precision in each step and gives the best result.

However, does $sign$ drive perturbations to the appropriate way? Probably not. Given typical attack method I-FGSM [2] as the baseline, in Figure 2 (a), we give a demonstration of the side-effect of sign in the $2D$ Euclidean space in the last step, where the origin O' of the coordinate is close to ℓ_∞ ϵ-ball. As shown in the figure, gradient $\boldsymbol{g}$ is extracted as two orthogonal direction, $\boldsymbol{u}$ and $\boldsymbol{v}$. Assuming original gradient is composed of $\boldsymbol{g} = 0.5\boldsymbol{u} + 0.1\boldsymbol{v}$. After sign, the value is exceptional modified to $\frac{\epsilon}{T}\boldsymbol{u} + \frac{\epsilon}{T}\boldsymbol{v}$, having the included angle

Y. Cheng, J. Song, X. Zhu, Q. Zhang, L. Gao, and H. T. Shen are with Center for Future Media and School of Computer Science and Engineering, University of Electronic Science and Technology of China, Chengdu, 611731, China (Email: yaya.cheng@hotmail.com)

Manuscript received XX.

0000–0000/00$00.00 © 2021 IEEE

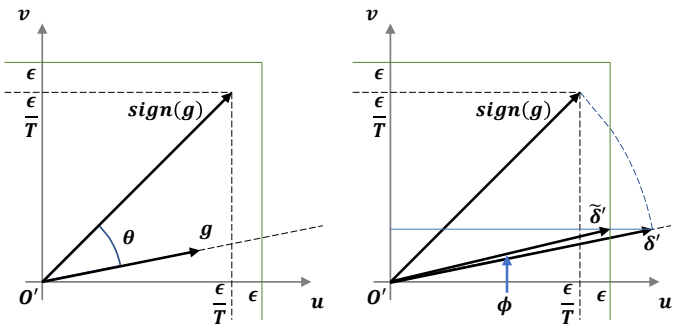


Fig. 2: Demonstration of the side-effect of sign operation in the $2D$ Euclidean space in the last step. (a): After sign, there exist a included angle $\angle\theta$ between gradient $\boldsymbol{g}$ and $\mathrm{sign}\,(\boldsymbol{g})$, (b): Our $\mathrm{FGNM_N}$ is done by firstly keeping magnitude same as $\mathrm{sign}\,(\boldsymbol{g})$, directions same as $\boldsymbol{g}$ and then being clipped. Easily verified in the figure, the included angle ϕ between $\tilde{\boldsymbol{\delta}}'$ and $\boldsymbol{g}$ is smaller than θ.

$\angle\theta = 33.7°$ between $\boldsymbol{g}$ and $\mathrm{sign}\,(\boldsymbol{g})$. Obviously, after $sign$, the direction of the perturbation is not strictly following the original gradient. Although $\mathrm{sign}\,(\boldsymbol{g})$ produces more perturbations under the ℓ_∞-norm scenario, it also introduces bias into the direction of perturbations. Since gradient is treated as the direction of fastest increase (untargeted) of $\mathcal{L}$ under the Euclidean feature space, the deviation in direction may make current gradient-based methods sub-optimal.

Therefore in this paper, we review the state-of-the-art attacks and give the correction on deviation in direction. Firstly, we introduce Taylor expansion to give a systematic analysis. Secondly, based on the analysis, our approach, Fast Gradient Non-sign Method is proposed, which completely replaces $sign$ with a refined one. Thirdly, by modifying the original algorithms as little as possible, such seamless replacement has been shown to boost all methods in the exhaustive experiments significantly. Figure 1 provides the toy example of climbing the mountain with three strategies to show the advantages of our FGNM. As demonstrated in the figure, noticed that the optima are inside the ϵ-ball, our two variants easily approach the optima. However, I-FGSM is stuck due to distorted perturbations. Specifically, when adopting I-FGSM, the trajectory is biased due to the limitation of sign. It can not approach the optima and results in oscillation. Our $\mathrm{I\text{-}FGNM_N}$ holds the identical step size with I-FGSM in each iteration, but produces a more precise trajectory and is close to the optima. The $\mathrm{I\text{-}FGNM_K}$ considers the trade-off between magnitude and precision of perturbations in each step and gives the best result.

Our contribution is summarized up as three folds:

1) Comprehensive analysis is conducted on the sign operation of gradient-based methods, which shows the bias between original gradients and the actual perturbations. As a result, this gap may hinder the abilities of current methods to maximize $\mathcal{L}$ and therefore needs further correction.

2) A general and novel routine, Fast Gradient Non-sign Methods are proposed to correct the currently adopted sign routines. With comprehensive analysis, our methods can obtain less gap between gradients and actual perturbations than previous ones, which brings us ability to obtain performance boosts.

3) Extensive experiments reveal the effectiveness of our methods. Specifically, for untargeted attacks, given normally trained models as black-box models, ours outperform state-of-the-art attacks by **27.5%** at most and **11.3%** on average. When transferring our adversarial examples to defense models, we still achieve a noticeable performance gain (*i.e.*, **25.8%** at most and **7.0%** on average). For targeted black-box attacks against defense models, our FGNM surpasses vanilla methods by **8.3%** on average and **18.5%** at most.

II. Related Works

Adversarial attacks are a rising topic in recent advances of artificial intelligence. Although neural networks go deeper and deeper, researchers find they are still vulnerable to specific inputs. In general, adversarial attacks can be classified into three categories: white-box, gray-box, and black-box attacks, which indicates how much information attackers can exploit from the victim's models. White-box attacks have achieved noticeable attack performance since they are able to get all information from the victim's models [19], [20]. For gray-box attacks, adversaries can only access the output logits or predictions, and adversarial examples are always crafted through huge amount queries [21], [22]. When all information from the victim's models is unavailable, it becomes the most challenging black-box attack, and current methods always suffer from poor effectiveness. We mainly focus on black-box attacks.

A. Black-box Attacks

Because the decision boundaries of different models are similar, an important property of adversarial examples is their transferability, *i.e.*, resultant adversarial examples generated from the white-box models are also effective for other models [23]. To tackle the poor performance of black-box attacks, several methods have been proposed to improve the transferability of adversarial examples [2]–[5], [7], [24]–[27]. For example, Goodfellow *et al*. [1] propose the fast gradient sign method to craft adversarial examples with just one step. I-FGSM [2] extends FGSM to an iterative attack and further improves the performance of white-box attacks at the cost of transferability. To further improve the transferability, by creating diverse patterns, DI-FGSM [4] finds adversarial examples which transfer better to black-box models. MI-FGSM [3] employs momentum term into the perturbation generation and achieves noticeable performance gains. TI-FGSM [5] optimizes a perturbation over an ensemble of translated images and achieves translation-invariant attacks. SI-FGSM [24] crafts more transferable adversarial examples with the help of the scale copies of inputs.

B. Defending against adversarial attacks

Good transferability of adversarial examples enables black-box attacks feasible in physical world [12]–[14], [28]–[33]. Consequently, a variety of defense methods have been proposed

to evade the threat of adversarial attacks. Characterized by defense approach, there are several main defense methods. Gradient masking [34]–[36] which hinders attackers from obtaining true gradients, are mainly proposed to protect models from optimization-based attacks. Auxiliary detection models [37] usually need to elaborate auxiliary models for predicting whether input is legitimate or adversarial. Other defense strategies will resort to preprocessing, *e.g.*, image transformations [38]–[40], denoising techniques [41], [42]. Some statistical methods [43] consider distribution of clean and adversarial samples as inconsistent. Therefore they usually detect adversarial examples with the help of statistics for distribution comparison. Defenses based on an ensemble of classifiers [44] are approaches formed by several classifiers. Adversarial training, one of the most powerful defenses methods, trains models to be more robust to adversarial attacks by introducing adversarial examples into dataset [44], [45].

III. Methodology

In this paper, we mainly discuss non-targeted attacks, and their targeted version can be simply derived [1]. Formally, given arbitrary input image $\boldsymbol{x} \in \mathbb{R}^{H\times W\times C}$ with ground-truth label y, non-targeted adversarial example $\boldsymbol{x}^{adv}$ aims at maximizing loss function $\mathcal{L}\left(\boldsymbol{x}^{adv}, y\right)$ under the ℓ_p norm constraint:

$$\begin{aligned} &\arg\max_{\boldsymbol{x}^{adv}} \mathcal{L}\left(\boldsymbol{x}^{adv}, y\right), \\ &s.t. \left\|\boldsymbol{x}^{adv} - \boldsymbol{x}\right\|_p \leq \epsilon. \end{aligned} \tag{1}$$

To measure the human-imperceptibility of adversarial examples, following previous works [2]–[5], [7], [24], ℓ_∞-norm is adopted in our work [2]. Specifically, when $p = \infty$, $\max|\boldsymbol{x}^{adv} - \boldsymbol{x}| \leq \epsilon$.

Some gradient-based attack methods [2], [3], [5] have been proposed to solve the optimization problem (1), *e.g.*, I-FGSM performs T-step attack with a small step size $\alpha = \epsilon/T$:

$$\begin{aligned} &\boldsymbol{x}_0^{adv} = \boldsymbol{x},\ \boldsymbol{g}_t = \nabla_{\boldsymbol{x}_t^{adv}} \mathcal{L}\left(\boldsymbol{x}_t^{adv}, y\right), \\ &\boldsymbol{x}_{t+1}^{adv} = \mathrm{clip}_\epsilon^{\boldsymbol{x}}\left(\boldsymbol{x}_t^{adv} + \alpha \cdot \mathrm{sign}\left(\boldsymbol{g}_t\right)\right), 0 \leq t < T, \end{aligned} \tag{2}$$

where sign operation makes perturbations meet the ℓ_∞-norm bound as soon as possible, and clip operation is performed to make $\boldsymbol{x}^{adv}$ satisfy the ϵ-ball of $\boldsymbol{x}$. Specifically:

$$\begin{aligned} \mathrm{sign}\left(\cdot\right) &= \begin{cases} +1 & \cdot > 0 \\ 0 & \cdot = 0 \\ -1 & \cdot < 0 \end{cases} \\ \mathrm{clip}_\epsilon^{\boldsymbol{x}}\left(\cdot\right) &= \min\left(\max\left(\cdot, \boldsymbol{x} - \epsilon\right), \boldsymbol{x} + \epsilon\right). \end{aligned} \tag{3}$$

Adopting basic pipeline of I-FGSM, other iterative methods are arranged into similar formulations, where the basic idea is generalized: performing method-specific manipulation on gradients $\boldsymbol{g}_t$ and then generating perturbations by sign operation.

[1] As adversarial examples generation pipelines of targeted and untargeted attacks are basically identical, later analysis of untargeted attacks is also adapted to targeted attacks. We omit to discuss targeted attacks for simplicity.

[2] For case of ℓ_2-norm please see III-D

A. Taylor Expansion of Loss Function

To theoretically solve the optimization problem, *i.e.*, Equation (1), we derive the first-order Taylor polynomial of $\mathcal{L}$ at the point $\boldsymbol{x}_{T-1}^{adv}$ as:

$$\begin{aligned} \mathcal{L}\left(\boldsymbol{x}_T^{adv}, y\right) &= \mathcal{L}\left(\boldsymbol{x}_{T-1}^{adv}, y\right) + \left(\boldsymbol{x}_T^{adv} - \boldsymbol{x}_{T-1}^{adv}\right) \cdot \nabla \mathcal{L}\left(\boldsymbol{x}_{T-1}^{adv}, y\right) + \mathcal{R}_1 \\ &= \mathcal{L}\left(\boldsymbol{x}, y\right) + \sum_{t=0}^{T-1} \left(\boldsymbol{x}_{t+1}^{adv} - \boldsymbol{x}_t^{adv}\right) \cdot \boldsymbol{g}_t + \mathcal{R}_1, \end{aligned} \tag{4}$$

where $\mathcal{R}_1$ is the remainder of first order and $\boldsymbol{g}_t = \nabla \mathcal{L}\left(\boldsymbol{x}_t^{adv}, y\right)$. Under the ℓ_∞-norm constraint, we assume $\boldsymbol{x}_{t+1}^{adv} - \boldsymbol{x}_t^{adv}$ is so small that $\mathcal{R}_1$ can be neglected. By denoting $\boldsymbol{x}_{t+1}^{adv} - \boldsymbol{x}_t^{adv} = \boldsymbol{\delta}_t$, Equation (4) is rewritten as:

$$\mathcal{L}\left(\boldsymbol{x}_T^{adv}, y\right) = \mathcal{L}\left(\boldsymbol{x}, y\right) + \sum_{t=0}^{T-1} \left\|\boldsymbol{\delta}_t\right\| \left\|\boldsymbol{g}_t\right\| \cos\left\langle\boldsymbol{\delta}_t, \boldsymbol{g}_t\right\rangle. \tag{5}$$

Obviously, $\sum_{t=0}^{T-1} \left\|\boldsymbol{\delta}_t\right\| \left\|\boldsymbol{g}_t\right\| \cos\left\langle\boldsymbol{\delta}_t, \boldsymbol{g}_t\right\rangle$ is the key component for maximizing $\mathcal{L}\left(\boldsymbol{x}_{t+1}^{adv}, y\right)$, where $\left\|\boldsymbol{\delta}_t\right\|$, $\boldsymbol{g}_t$ is the magnitude of noises, gradient at iteration t. $\left\langle\boldsymbol{\delta}_t, \boldsymbol{g}_t\right\rangle$ is the included angle between $\boldsymbol{\delta}_t$ and $\boldsymbol{g}_t$. Although $\left\|\boldsymbol{g}_t\right\|$ also affects the results, we treat it identical in different trajectories by assuming loss function is smooth and gradient does not change rapidly in a small region.

B. Drawbacks of Sign-based Attacks

As mentioned above, $\boldsymbol{g}_t$ indicates the direction of pulling $\boldsymbol{x}_t^{adv}$ to increase $\mathcal{L}$. However, considering that sign coarsely quantifies gradients to $\{+1, -1, 0\}$, there always exists a bias of direction between the perturbation and gradients. As Figure 3 demonstrates, sign method pushes the point far away from the optima, which indicates the side-effect of this biased gradient manipulation. Based on the analysis in Sec. III-A, in following sections we will explain why adopting sign will make Equation (5) sub-optimal and give our approach.

For simplicity, we hypothesize $\boldsymbol{g_t}$ is non-zero. $\boldsymbol{x}_t^{adv}$ and $\boldsymbol{g}_t$ are interpreted as flattened vectors with dimension $D = H \times W \times C$:

$$\begin{aligned} \boldsymbol{x}_t^{adv} &= \left[x^1, x^2, \cdots, x^D\right]_t, \\ \boldsymbol{g}_t &= \left[\nabla_{x^1}, \nabla_{x^2}, \cdots, \nabla_{x^D}\right]_t. \end{aligned} \tag{6}$$

To make the derivation simple, we select the typical sign-based attack: I-FGSM as our baseline. Then, $\boldsymbol{\delta}_t = \mathrm{sign}\left(\boldsymbol{g}_t\right)$ and $\cos\left\langle\boldsymbol{\delta}_t, \boldsymbol{g}_t\right\rangle$ is denoted as $\cos\theta_t$, where:

$$\cos\theta_t = \frac{\boldsymbol{g}_t \cdot \mathrm{sign}\left(\boldsymbol{g}_t\right)}{\left\|\boldsymbol{g}_t\right\| \left\|\mathrm{sign}\left(\boldsymbol{g}_t\right)\right\|} = \frac{\left\|\boldsymbol{g}_t\right\|_1}{\sqrt{\left\|\boldsymbol{g}_t\right\|_0} \left\|\boldsymbol{g}_t\right\|}. \tag{7}$$

Here, $\left\|\boldsymbol{g}_t\right\|_1 = \sum|\boldsymbol{g}_t^j|$, $\left\|\boldsymbol{g}_t\right\|_0 = D$. Due to the fact that $\left\|\cdot\right\|_1 \geq \left\|\cdot\right\|$ for any vector and $\left\|\cdot\right\|_1 = \left\|\cdot\right\|$ *iff* the vector is all zero or it only has one non-zero entry, $\cos\theta$ ranges in:

$$\frac{1}{\sqrt{D}} < \cos\theta \leq 1. \tag{8}$$

Obviously,

$$\left\|\boldsymbol{\delta}_t\right\| = \alpha\sqrt{D} \tag{9}$$

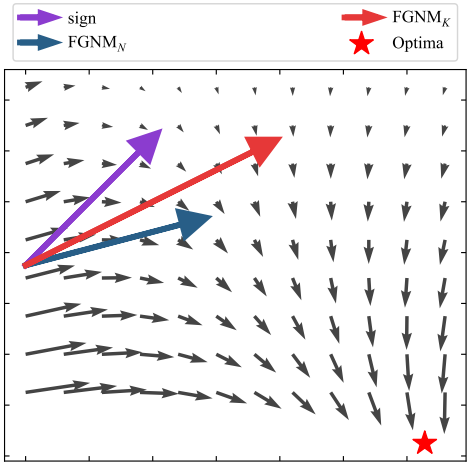


Fig. 3: Quiver plot for visualizing gaps between original gradients and actual perturbations in the demo scenario. To approach optima in the fastest way, a step's magnitude and direction are vital components. In this figure, our FGNM$_{\mathrm{N}}$ and FGNM$_{\mathrm{K}}$ take the right step at the starting point. However, the sign method goes far away instead.

$$\alpha < \|\boldsymbol{\delta}_t\| \cos\theta \leq \alpha\sqrt{D}. \tag{10}$$

Two special cases will make $\cos\theta = 1$: a) $D = 1$, or b) All values of $\boldsymbol{g}_t$ are identical, which makes $\|\boldsymbol{g}_t\|_1 = \sqrt{D}\,\|\boldsymbol{g}_t\|$.

The derivation of θ_t indicates the gap between real gradients and actual perturbations at current iteration i. In fact, special cases mentioned above are nearly impossible to approach in practice, especially in high-dimensional space. Therefore the ideal maximum of $\|\boldsymbol{\delta}_t\| \cos\theta_t$ is difficult to achieve, and we usually seek the sub-optimal solution of Equation (4).

C. Fast Gradient Non-sign Methods

1) Fixed Scale Approach: To reduce the side-effect caused by sign, Iterative Fast Gradient Non-sign Method (I-FGNM) and other variants are proposed. To distinguish our method, we denote the magnitude of our noise as $\|\boldsymbol{\delta'}\|$ and the included angle as ϕ. An intuitive solution is to perform a linear scale on the $\boldsymbol{g}_t$ so that $\|\boldsymbol{\delta'}\| = \|\mathrm{sign}\,(\boldsymbol{g}_t)\|$ and naturally $\cos\phi = 1 \geq \cos\theta$. To achieve this, a scale factor ζ is defined as:

$$\zeta = \frac{\|\mathrm{sign}(\boldsymbol{g}_t)\|}{\|\boldsymbol{g}_t\|}, \quad \boldsymbol{\delta'_t} = \alpha \cdot \zeta \cdot \boldsymbol{g}_t. \tag{11}$$

We call this simple solution as I-FGNM$_{\mathrm{N}}$ since the norm between $\boldsymbol{\delta'}$ and $\mathrm{sign}\,(\boldsymbol{g})$ are equal.

Empirically in iterative algorithms, the step size α is much smaller than ϵ. So in the first few steps, our noises are too small to be clipped. We have:

$$\|\boldsymbol{\delta}_t\| \cos\theta_t \leq \left\|\boldsymbol{\delta'_t}\right\| \cos\phi_t = \alpha\sqrt{D}. \tag{12}$$

The derivation shows that $\mathcal{L}$ calculated from our approach will always be greater or equal than the sign approach, according to Equation (12) and (5) if there is no clipping. However, in the last few steps, the accumulated noises of previous steps make $\boldsymbol{x}_t^{adv}$ close to the ϵ-ball, and it will be more likely to be clipped. In this scenario, the actual noises added in the t-th iteration will be:

$$\boldsymbol{x}_{t+1}^{adv} - \boldsymbol{x}_t^{adv} = \mathrm{clip}_{\epsilon}^{\boldsymbol{x}}\left(\boldsymbol{x}_t^{adv} + \alpha \cdot \boldsymbol{\delta'_t}\right) - \boldsymbol{x}_t^{adv}. \tag{13}$$

Clipping introduces biases, *i.e.*, $\left\|\boldsymbol{\delta'_t}\right\|$ decreases and $\cos\phi_t$ will be smaller than 1. It is complicated to judge the clipped $\boldsymbol{\delta'_t}$ and δ_t which one is better. And instead, we analyze it in a qualitative way. The clipped $\boldsymbol{\delta'_t}$ contains two parts: The non-clipped component and clipped component. If we only consider the non-clipped one, it still preserves the original gradients and performs linear scale. On the contrary, the clipped one only contains $-\epsilon$ or $+\epsilon$. So we treat it as ***partially distorted***. Different from $\mathrm{sign}\,(\boldsymbol{g}_t)$ which is ***fully distorted***, our mixed vector is more likely to be closed to $\boldsymbol{g}_t$ than $\mathrm{sign}\,(\boldsymbol{g}_t)$. Figure 2 demonstrates the analysis on clipping. As the figure shows, the $\boldsymbol{u}$-component of $\boldsymbol{\delta'}$ is reduced to ϵ while the $\boldsymbol{v}$-component of $\boldsymbol{\delta'}$ is preserved. The actual perturbation is denoted as $\tilde{\boldsymbol{\delta}}'$. Easily verified in the figure, the scaled and clipped result $\tilde{\boldsymbol{\delta}}'$ is closer to $\boldsymbol{g}_t$. Overall, $\sum_{t=0}^{T}\left\|\tilde{\boldsymbol{\delta}}'_{\boldsymbol{t}}\right\| \cos\phi_t$ is larger than $\sum_{t=0}^{T}\|\boldsymbol{\delta}_t\| \cos\theta_t$.

2) Adaptive Scale Approach: Although I-FGNM$_{\mathrm{N}}$ is applicable for most cases by fixing $\left\|\boldsymbol{\delta'_t}\right\|$, the attack performance is not always guaranteed due to clipped ratio. Empirically, a large clipped ratio hinders the performance of I-FGNM$_{\mathrm{N}}$. To consider this ratio formally and comprehensively, we relax the constraint on $\left\|\boldsymbol{\delta'_t}\right\|$ and compose a heuristic method I-FGNM$_{\mathrm{K}}$, where the scale factor of I-FGNM$_{\mathrm{K}}$ is set by directly finding the proper value from all possible values:

$$\begin{aligned} scales &= \mathrm{Sort}\left(\frac{1}{|\boldsymbol{g}_t^k|}\right), \ \boldsymbol{g}_t^k \in \boldsymbol{g}_t, \\ \zeta &= scales\,[K]\,. \end{aligned} \tag{14}$$

Specifically, $scales$ are calculated and sorted from $1/|\boldsymbol{g}_t^k|$, then ζ is picked by the K-th *biggest* value of $scales$. As described before, two components (magnitude and direction of noise) essentially influence attack performance. For I-FGNM$_{\mathrm{K}}$, there exists a trade-off between the two components, which is influenced by controlling K. Intuitively, larger K leads to smaller magnitude, smaller clipped ratio, and larger $\cos\phi_t$. The Fast Gradient Non-sign Methods is summarized in Algorithm 1.

D. Discussion

Our Fast Gradient Non-sign Methods are delivered with two variants, FGNM$_{\mathrm{N}}$ and FGNM$_{\mathrm{K}}$. The former generates noises $\boldsymbol{\delta'}$ by linearly scaling from $\boldsymbol{g}$ and keeping the magnitude same as $\|\mathrm{sign}\,(\boldsymbol{g}_t)\|$ with a scale ζ. The latter relaxes the magnitude to consider the trade-off between $\|\boldsymbol{\delta'}\|$ and $\cos\phi$. Moreover, the replacement is seamless and universal. Any current FGSM-based attacks are applicable to become FGNM-based attacks, *e.g.*, MI-FGSM, TI-FGSM, DI-FGSM, SI-FGSM, and the computational overhead is negligible.

Noticed that there also exists another style of attack whose constraint is defined as $\left\|\boldsymbol{x}^{\boldsymbol{adv}} - \boldsymbol{x}\right\| \leq \epsilon$ (ℓ_2 attacks). We need to clarify the difference between our FGNM and ℓ_2 attacks. Firstly, since the constraint is changed, ℓ_2 attacks are not troubled by the ℓ_∞ constraint, which causes the gradients to be distorted. Secondly, our approaches essentially consider reducing the side-effect of sign operation to leverage the

Algorithm 1: Algorithms of I-FGNM

Input : A classifier $\mathcal{F}$ with loss function $\mathcal{L}$; input image $\boldsymbol{x}$ with ground-truth label y; T iterations; the size of perturbation ϵ;

Output : Adversarial example $\boldsymbol{x^{adv}}$ with $\left\|\boldsymbol{x}^{adv}-\boldsymbol{x}\right\|_\infty \leq \epsilon$;

Initialize: $\boldsymbol{x_0^{adv}}=\boldsymbol{x}$, $\alpha=\epsilon/T$

$t \leftarrow 0$;

while $t < T$ **do**

  /* generation loop of $\boldsymbol{x^{adv}}$ */

  Input $\boldsymbol{x_t^{adv}}$ to $\mathcal{L}$ and obtain the gradient $\boldsymbol{g}_t=\nabla_{\boldsymbol{x}}\mathcal{L}\left(\boldsymbol{x}_t^{adv},y\right)$;

  Calculate ζ by Equation (11) or Equation (14);

  Update $\boldsymbol{x}_{t+1}^{adv}$ by our non-sign operation as $\boldsymbol{x}_{t+1}^{adv}=\boldsymbol{x}_t^{adv}+\alpha\cdot\zeta\cdot\boldsymbol{g}_t$;

  $t \leftarrow t+1$;

end

TABLE I: Hyper-parameters adopted in our experiments for MI-FGSM, DI-FGSM, TI-BIM, and SI-FGSM, respectively. For a fair comparison, our methods use identical hyper-parameters.

Methods	Hyper-parameters	Value	
MI-FGSM	Momentum μ	1.0	
DI-FGSM	Transform probability p	0.7	
TI-BIM	Kernel length W	Untargeted	15
		Targeted	5
SI-FGSM	Number of the scale copies c	5	

performance of ℓ_∞ attacks finally. Therefore, we believe our approaches have advantages among the ℓ_∞ attacks.

IV. Experiments

To confirm our analysis and compare with currently state-of-the-art attacks, extensive experiments are conducted in non-targeted and targeted ℓ_∞ attack scenario.

A. Setup

a) Dataset: The ImageNet-compatible dataset in the NIPS 2017 adversarial competition[3] is chosen to evaluate our methods and state-of-the-art attacks. This dataset contains $1,000$ images and is widely used in previous works [3], [5], [6], [24].

b) Models: To give comprehensive statistical analysis, experiments are conducted on eight models, including five normally trained models (NT): Inception V3 (Inc-v3) [46], Inception V4 (Inc-v4) [47], ResNet152 V2 (Res152) [48], Inception-Resnet V2 (IncRes) [49] and DenseNet 161 (Den161) [50], and three ensemble adversarially trained models (EAT): Inc-v3$_{ens3}$, Inc-v3$_{ens3}$ and IncRes$_{ens}$ [44].

c) Baselines: As described above, our FGNM are applicable for any FGSM-based methods by directly replacing sign with scale ζ. In this paper, six currently popular FGSM-based attacks are selected as baselines: I-FGSM [2], MI-FGSM [3], DI-FGSM [4], TI-BIM [5], PoI-FGSM [7] and SI-FGSM [24]. Our boosted versions are denoted as I-FGNM, MI-FGNM, DI-FGNM, TI-BNIM, PoI-FGNM, SI-FGNM, respectively. Both two variants (FGNM$_{\text{N}}$ and FGNM$_{\text{K}}$) are evaluated.

d) Hyper-parameters: To make a fair comparison, we follow the previous works [3]–[5], [24] to set hyper-parameters. For the generalized parameters, we set $\epsilon=16$ with pixel-level ranges in $0\sim255$. And for untargeted iterative method, the total iteration number T and step size α are 10 and $\epsilon/10=1.6$, respectively. For targeted iterative method, they are 20 and $\epsilon/20=0.8$. As for method-specific hyper-parameters, we adopt the original value reported in their paper, as shown in Table I. Note that our methods will not modify these hyper-parameters.

[3]https://www.kaggle.com/c/nips-2017-non-targeted-adversarial-attack

B. Effectiveness of K

In this section, we firstly study the effectiveness of K since it represents the trade-off between magnitude and bias of noises.

To find an appropriate K, given Inc-v3 as white-box models and K ranging from 1 to $299\times299\times3$ with interval 500, we firstly craft untargeted adversarial examples using all FGNM$_{\text{K}}$-based methods and then report the average attack success rate against black-box NT and EAT in Figure 4 and Figure 5 respectively. We also plot the performance of sign-based methods and our FGNM$_{\text{N}}$ methods, which will be discussed in the next sections. As demonstrated from the vast majority of concave curves in Figure 4 and Figure 5. As for NT, we give a unified optimal K for all methods $K=120,000$. For EAT, $K=200,000$.

A natural question is that why most of the curves corresponding to our FGNM$_{\text{K}}$ in Figure 4 and Figure 5 are concave. In particular, we pick I-FGNM$_{\text{K}}$ to answer this question. As described before, magnitude and bias of noises play a key role in performing successful attack. Therefore, a potential reason for the concave trends is analysis of these two components in Sec III-C1. To confirm the analysis in Sec III-C1, we measure these two values on I-FGNM$_{\text{K}}$. To obtain actual noises added in the i-th iteration, we compute $\boldsymbol{\delta}_t'=\boldsymbol{x}_{t+1}^{adv}-\boldsymbol{x}_t^{adv}$. Then, magnitude is computed by $\left\|\boldsymbol{\delta}_t'\right\|$ and bias of direction is computed by $\cos\phi_t=\frac{\langle\boldsymbol{\delta}_t',\boldsymbol{g}_t\rangle}{\|\boldsymbol{\delta}_t'\|\|\boldsymbol{g}_t\|}$ and they are averaged among whole iterations. The results with respect to K are placed in Figure 6. This figure shows our idea for presenting the trends of $\|\boldsymbol{\delta'}\|$ and $\cos\phi$ when varying K. Particularly, when K increases, the scale ζ decreases, and therefore the generated perturbations will be smaller. Meanwhile, smaller perturbations leads to a smaller clipped ratio, and instead preserves the direction. So the actual $\|\boldsymbol{\delta'}\|$ goes down while $\cos\phi$ goes up. Naturally, there exists a maximum value of $\|\boldsymbol{\delta'}\|\cos\phi$.

C. Comparisons with State-of-the-Art Attacks

1) Performance of untargeted attacks: After finding the optimal K, comprehensive experiments are conducted further to evaluate the effectiveness of our methods against NT and EAT under untargeted setting.

a) Attack against Normally Trained Models: In this section, we study the vulnerability of NT w.r.t different algorithms, including FGNM$_{\text{N}}$-based, FGNM$_{\text{K}}$-based, and their corresponding FGSM-based methods. Adversarial examples are crafted via given white-box models by different methods.

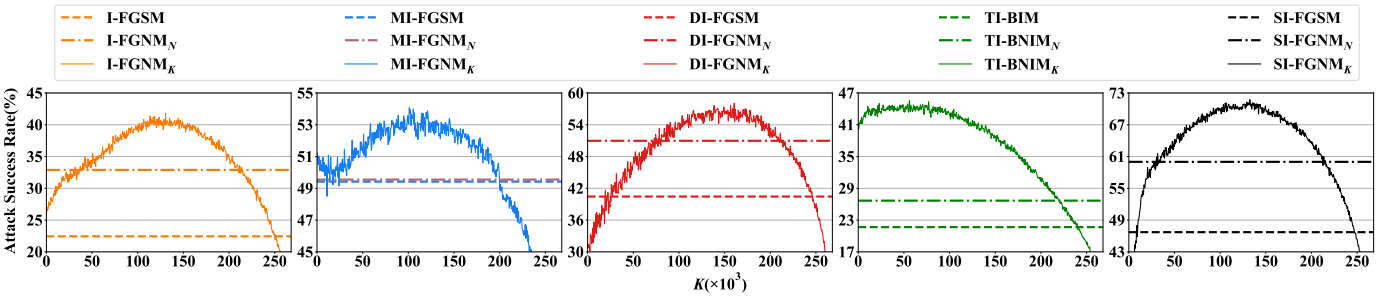


Fig. 4: Average untargeted attack success rate comparisons between sign methods and our FGNM_K variants on normally trained models. We employ Inc-v3 as white-box and compute average attack success rate of other four black-box models (Inc-v4, Res152, IncRes, and Den161) w.r.t. K. Results of sign-based methods and FGNM_N variants are also reported as dashed lines and dash-dotted lines, respectively.

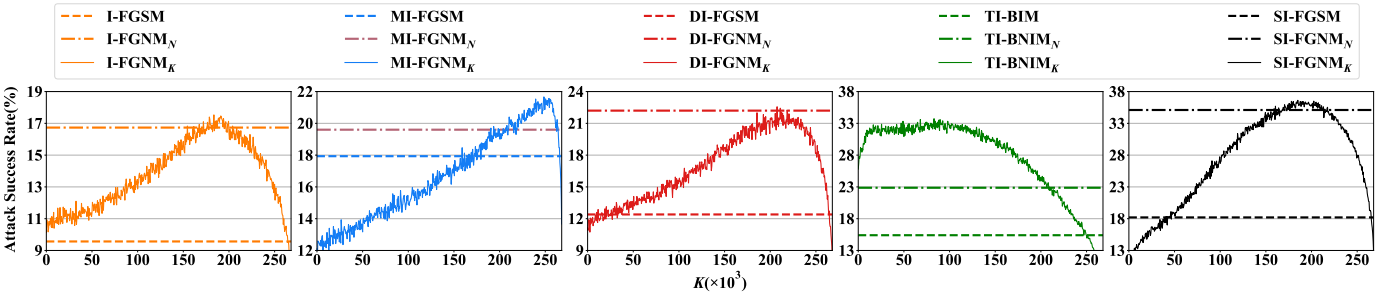


Fig. 5: Average untargeted attack success rate comparisons between sign methods and our FGNM_K variants on adversarially trained models. We employ Inc-v3 as white-box and compute average attack success rate of three black-box models ($\text{Inc-v3}_{\text{ens3}}$, $\text{Inc-v3}_{\text{ens4}}$, $\text{IncRes}_{\text{ens}}$) w.r.t. K. Unlike NT, the best results present in the later area in most cases. Results of sign-based methods and FGNM_N variants are also reported as dashed lines and dash-dotted lines, respectively.

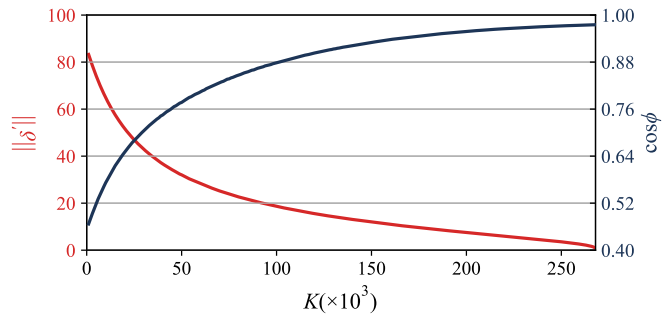


Fig. 6: Evaluation on average $\cos\phi$ and $\|\delta'\|$ w.r.t. K to show the changes of magnitude and direction of added perturbations. Obviously, $\|\delta'\|$ decreases when K increases, and $\cos\phi$ goes up in contrast. The trends confirm our analysis of magnitude and direction of noises.

As shown in Table II, FGNM_N and FGNM_K sustain powerful white-box attack performance since they achieve near 100% success rate against all white-box models. For black-box attacks, our methods are applicable to most attacks, such as I-FGSM, DI-FGSM, TI-BIM, SI-FGSM. Specifically, by integrating FGNM_N with them, our methods surpass I-FGSM, DI-FGSM, TI-BIM, SIFGSM in the black-box manner by a large margin, *i.e.*, on average, **9.8%**, **8.6%**, **6.8%**, **11.4%** respectively. For MI-FGNM_N, which is based on cumulative gradients, the gradients are so large that most of the pixels will be clipped if applying FGNM_N to them, and therefore no noticeable performance leverage is obtained by MI-FGNM_N compared with MI-FGSM. By integrating FGNM_K with each FGSM-based method, our methods outperform I-FGSM, MI-FGSM, DI-FGSM, TI-BIM, SI-FGSM for the black-box attacks by **18.7%**, **3.3%**, **14.1%**, **20.3%**, **20.7%**.

b) Attack against Defense Models: Adversarial training technique is an effective way to evade attacks, especially for black-box attacks. Nevertheless, we still obtain expected results. As placed in Table III, our FGNM_N and FGNM_K achieve the best performance in most cases, especially for I-FGNM_K, DI-FGNM_N, TI-BNIM_K, and SI-FGNM_K, which outperform vanilla methods by **12.0%**, **17.2%**, **13.3%** and **26.4%** on average. Results among MI variants are also satisfied, where our MI-FGNM_N obtains **4.2%** performance gain on average.

Experiment results demonstrate that in most cases, our fixed scale approach FGNM_N reduces the side effects of sign operation and improves the transferability of adversarial examples. Our adaptive scale approach FGNM_K relaxes restrictions added by FGNM_N with the noise magnitude, adaptively adjusts scale factor, and further improves the attack performance. It is noticeable that performance gap between our FGNM_N and FGNM_K variants is smaller on EAT than NT. Intuitively, due to decision boundaries between EAT and NT being more different than that between NT, adversarial examples generated on NT

TABLE II: Quantitative comparisons between state-of-the-art attacks on normally trained models. Specifically, Inc-v3, Inc-v4, Res152 and IncRes are adopted to craft untargeted adversarial examples respectively. "*" denotes the white-box results while others are black-box results.

Models	Attacks	Inc-v3	Inc-v4	Res152	IncRes	Den161	Models	Inc-v3	Inc-v4	Res152	IncRes	Den161
Inc-v3	I-FGSM	**100.0***	29.4	18.9	20.3	21.2	Inc-v4	42.0	**100.0***	22.6	25.8	24.4
	I-FGNM$_N$ (ours)	**100.0***	41.9	28.2	33.4	28.1		51.5	**100.0***	32.2	35.5	31.0
	I-FGNM$_K$ (ours)	**100.0***	**48.7**	**32.7**	**44.2**	**36.5**		**63.0**	**100.0***	**40.4**	**46.0**	**44.3**
	MI-FGSM	**100.0***	55.1	43.0	50.9	48.7		70.8	**100.0***	52.2	59.0	55.5
	MI-FGNM$_N$ (ours)	**100.0***	56.2	42.8	52.3	46.9		69.7	**100.0***	50.0	58.2	52.3
	MI-FGNM$_K$ (ours)	**100.0***	**59.0**	**45.9**	**57.9**	**51.1**		**74.3**	**100.0***	**54.0**	**63.3**	**56.5**
	DI-FGSM	99.9*	54.9	33.6	41.7	31.6		64.9	**100.0***	39.1	49.4	37.2
	DI-FGNM$_N$ (ours)	99.7*	65.3	43.7	55.1	39.8		73.7	**100.0***	47.8	59.4	45.2
	DI-FGNM$_K$ (ours)	**100.0***	**67.3**	**45.6**	**62.0**	**47.0**		**78.4**	**100.0***	**55.0**	**66.4**	**54.5**
	TI-BIM	99.9*	28.1	16.7	13.5	28.4		35.2	**100.0***	20.4	17.0	31.8
	TI-BNIM$_N$ (ours)	**100.0***	25.9	23.3	23.9	33.6		46.3	**100.0***	27.4	26.7	40.2
	TI-BNIM$_K$ (ours)	**100.0***	**47.4**	**33.6**	**35.9**	**47.6**		**58.2**	**100.0***	**35.6**	**39.4**	**54.7**
	SI-FGSM	**99.0***	53.8	40.4	47.8	44.9		72.6	**100.0***	51.0	57.0	57.2
	SI-FGNM$_N$ (ours)	**99.0***	67.7	52.7	63.2	56.4		78.0	**100.0***	61.3	70.8	65.1
	SI-FGNM$_K$ (ours)	**99.0***	**76.6**	**64.1**	**73.2**	**67.0**		**86.4**	**100.0***	**71.9**	**77.9**	**76.6**
Res152	I-FGSM	31.4	25.1	**99.5***	17.0	23.8	IncRes	46.2	38.6	27.6	**100.0***	28.1
	I-FGNM$_N$ (ours)	40.8	35.3	99.1*	30.5	34.3		56.6	49.3	35.7	99.9*	35.8
	I-FGNM$_K$ (ours)	**52.0**	**46.6**	**99.5***	**42.4**	**44.9**		**65.6**	**53.8**	**39.0**	**100.0***	**43.5**
	MI-FGSM	56.1	50.8	**99.5***	47.2	54.6		76.4	67.8	57.0	**100.0***	60.3
	MI-FGNM$_N$ (ours)	55.7	49.6	**99.5***	46.2	52.7		75.2	65.6	55.2	**100.0***	58.3
	MI-FGNM$_K$ (ours)	**62.6**	**56.7**	**99.5***	**53.9**	**58.0**		**77.0**	**69.2**	**58.6**	**100.0***	**61.2**
	DI-FGSM	62.1	55.6	99.1*	49.4	47.4		70.6	66.7	48.1	99.5*	45.1
	DI-FGNM$_N$ (ours)	69.9	64.2	99.3*	58.7	56.5		76.9	74.3	56.3	99.6*	51.9
	DI-FGNM$_K$ (ours)	**76.2**	**70.1**	**99.6***	**67.1**	**64.8**		**80.6**	**76.8**	**56.8**	**98.8***	**57.8**
	TI-BIM	24.7	21.3	99.2*	11.5	30.9		44.0	40.2	26.3	99.4*	41.0
	TI-BNIM$_N$ (ours)	33.1	27.8	99.0*	19.1	35.9		51.0	45.4	30.5	**99.6***	46.5
	TI-BNIM$_K$ (ours)	**47.0**	**41.6**	**99.5***	**33.3**	**54.2**		**63.0**	**56.5**	**43.1**	99.0*	**61.6**
	SI-FGSM	43.6	40.0	**99.8***	30.6	44.6		72.8	63.9	52.7	99.9*	58.8
	SI-FGNM$_N$ (ours)	53.9	48.9	99.7*	53.9	56.3		81.3	73.5	64.6	99.9*	67.7
	SI-FGNM$_K$ (ours)	**66.0**	**62.6**	**99.8***	**58.1**	**68.6**		**86.6**	**80.6**	**70.7**	**100.0***	**75.4**

TABLE III: Quantitative comparisons between state-of-the-art attacks on adversarially trained models (EAT). Inc-v3, Inc-v4, Res152, and IncRes are adopted as white-box models to generate untargeted adversarial examples, while EAT are used to test transferability of adversarial examples.

	Inc-v3			Inc-v4			Res152			IncRes		
Attacks	Inc-v3$_{ens3}$	Inc-v3$_{ens4}$	IncRes$_{ens}$	Inc-v3$_{ens3}$	Inc-v3$_{ens4}$	IncRes$_{ens}$	Inc-v3$_{ens3}$	Inc-v3$_{ens4}$	IncRes$_{ens}$	Inc-v3$_{ens3}$	Inc-v3$_{ens4}$	IncRes$_{ens}$
I-FGSM	12.1	12.6	4.6	12.0	12.0	5.8	12.3	13.4	6.7	13.3	12.8	8.9
I-FGNM$_N$ (ours)	**18.9**	**20.8**	10.5	18.7	19.5	11.6	21.7	22.5	15.5	26.2	23.8	18.4
I-FGNM$_K$ (ours)	18.5	20.1	**10.6**	**19.9**	**20.7**	**12.2**	**22.4**	**23.9**	**16.1**	**26.3**	**24.2**	**19.2**
MI-FGSM	22.2	21.2	10.4	24.6	22.4	13.4	24.7	26.7	15.7	31.2	28.6	20.7
MI-FGNM$_N$ (ours)	**22.8**	23.2	**12.8**	**26.3**	**26.4**	**16.1**	31.0	**30.0**	**19.0**	**36.5**	**32.1**	**25.7**
MI-FGNM$_K$ (ours)	21.9	**23.3**	11.9	25.3	25.2	14.7	**31.2**	28.7	18.4	34.6	31.5	23.0
DI-FGSM	14.2	15.7	7.3	14.6	16.8	9.4	21.0	20.9	12.4	20.8	18.7	12.3
DI-FGNM$_N$ (ours)	**24.7**	**27.0**	**14.9**	**27.3**	26.0	17.1	**38.1**	**36.2**	26.4	**38.3**	34.7	**28.5**
DI-FGNM$_K$ (ours)	24.3	26.7	13.4	27.0	**26.7**	**17.3**	37.7	35.1	**26.6**	37.8	**35.0**	27.1
TI-BIM	17.5	18.0	10.7	17.2	20.4	11.8	18.5	18.7	12.6	25.4	25.8	21.1
TI-BNIM$_N$ (ours)	25.6	25.9	17.1	28.5	28.3	19.8	25.3	25.4	19.7	37.4	35.9	30.6
TI-BNIM$_K$ (ours)	**27.3**	**27.3**	**18.8**	**29.1**	**28.4**	**20.4**	**27.9**	**29.0**	**21.3**	**37.7**	**37.0**	**33.8**
SI-FGSM	21.7	22.5	10.4	27.3	28.5	16.9	20.2	18.7	12.3	30.0	28.2	21.6
SI-FGNM$_N$ (ours)	38.8	41.1	**25.4**	49.6	48.5	**33.2**	37.0	34.6	27.3	54.3	48.3	45.7
SI-FGNM$_K$ (ours)	**40.0**	**42.4**	25.3	**50.9**	**49.0**	32.2	**37.9**	**37.8**	**27.4**	**55.8**	**50.5**	**46.4**

are more challenging to transfer to EAT, *i.e.*, smaller gap. Similarly, differences in decision boundaries between EAT and NT result in different attack performance against them using the same K, *i.e.*, different trends w.r.t. K in Figure 4 and 5.

c) Effectiveness on Combination of Methods: To further verify the effectiveness of our methods, we also report the results on different combinations of methods: DTI-FGSM, DSI-FGSM, DTSI-FGSM, MDTSI-FGSM, and their FGNM$_N$, FGNM$_K$ variants. Specifically, we firstly attack given white-box models using different methods and then transfer resultant adversarial examples to black-box models, including NT and EAT. As demonstrated in Table. IV and V, our FGNM$_N$ and FGNM$_K$ substantially improve the transferability of black-box attacks without sacrificing the effectiveness of white-box attacks. In most cases, noticeable black-box attack performance gain is achieved by just applying our FGNM$_N$ to original methods, with an average of **4.1%**, **9.9%** and a maximum of **11.8%**, **24.9%** for NT and EAT, respectively. The most powerful attacks come from FGNM$_K$ variants. For black-box NT, our FGNM$_K$ variants outperform state-of-the-art attacks by **11.1%** on average and **24.6%** at most. For EAT, FGNM$_K$ variants achieve comparable results of FGNM$_N$ variants, which outperforms state-of-the-art attacks by **24.8%** at most and **11.3%** on average. Significant performance improvement on the combined version of attack methods confirms the universality and effectiveness of our approach.

2) Performance of targeted attacks: To verify the performance of proposed FGNM$_N$ and FGNM$_K$, following setup

TABLE IV: Quantitative comparisons between different combinations of methods on normally trained models. Untargeted aversarial examples are crafted via Inc-v3, Inc-v4, Res152 and IncRes. The rest of models are used to verify transferability. "*" denotes the white-box results while others are black-box results.

Models	Attacks	Inc-v3	Inc-v4	Res152	IncRes	Den161	Models	Inc-v3	Inc-v4	Res152	IncRes	Den161
Inc-v3	DTI-FGSM	97.3*	45.1	25.5	25.3	41.0	Inc-v4	35.0	**100.0***	20.7	17.1	31.7
	DTI-FGNM$_N$ (ours)	97.5*	52.0	31.9	36.9	46.7		44.8	**100.0***	25.8	26.6	40.0
	DTI-FGNM$_K$ (ours)	**98.0***	**62.5**	**42.5**	**47.4**	**61.0**		**58.6**	**100.0***	**36.5**	**41.7**	**54.4**
	DSI-FGSM	**100.0***	83.9	67.6	76.0	70.6		88.2	99.6*	73.3	81.6	75.9
	DSI-FGNM$_N$ (ours)	**100.0***	87.5	75.1	83.2	77.1		90.9	**100.0***	77.1	87.2	81.3
	DSI-FGNM$_K$ (ours)	**100.0***	**90.9**	**80.4**	**87.5**	**83.5**		**92.9**	**100.0***	**83.7**	**89.3**	**87.9**
	DTSI-FGSM	99.7*	68.6	46.3	53.5	74.0		74.3	99.9*	48.7	60.1	77.5
	DTSI-FGNM$_N$ (ours)	99.9*	74.5	52.6	62.2	79.9		77.6	**100.0***	53.9	66.7	80.6
	DTSI-FGNM$_K$ (ours)	**100.0***	**82.1**	**61.5**	**69.4**	**86.3**		**84.1**	**100.0***	**63.0**	**71.1**	**87.8**
	MDTSI-FGSM	99.5*	77.2	59.9	63.4	84.0		80.3	99.7*	60.5	67.4	84.7
	MDTSI-FGNM$_N$ (ours)	99.7*	75.3	58.8	62.4	83.8		78.3	99.9*	60.0	66.1	84.6
	MDTSI-FGNM$_K$ (ours)	**99.9***	**80.4**	**64.6**	**67.7**	**88.1**		**83.1**	**100.0***	**65.0**	**71.5**	**88.1**
Res152	DTI-FGSM	45.1	40.4	97.9*	30.6	53.2	IncRes	42.3	39.3	25.8	99.4*	40.0
	DTI-FGNM$_N$ (ours)	52.2	51.3	98.4*	42.4	59.2		51.2	45.3	31.0	99.5*	46.7
	DTI-FGNM$_K$ (ours)	**63.9**	**59.8**	**99.2***	**53.5**	**73.5**		**63.4**	**58.2**	**42.6**	**99.7***	**50.2**
	DSI-FGSM	79.9	75.0	**99.9***	72.7	79.5		91.7	88.0	81.9	99.9*	82.7
	DSI-FGNM$_N$ (ours)	83.9	81.2	**99.9***	79.8	83.7		92.6	90.4	83.7	99.8*	84.8
	DSI-FGNM$_K$ (ours)	**88.8**	**86.9**	**99.9***	**84.8**	**89.6**		**94.6**	**92.9**	**87.3**	**100.0***	**88.8**
	DTSI-FGSM	61.3	58.9	98.8*	54.1	79.6		81.4	80.6	65.6	98.9*	87.4
	DTSI-FGNM$_N$ (ours)	66.8	66.7	99.0*	61.6	81.4		83.6	81.0	68.2	99.3*	88.4
	DTSI-FGNM$_K$ (ours)	**76.7**	**74.0**	**99.9***	**69.4**	**89.5**		**88.1**	**87.3**	**76.0**	**99.8***	**92.9**
	MDTS-FGSM	67.3	65.3	98.2*	60.7	83.6		81.2	79.5	70.3	98.1*	88.8
	MDTSI-FGNM$_N$ (ours)	67.3	64.1	98.9*	61.3	83.1		82.1	79.8	69.1	98.7*	88.1
	MDTSI-FGNM$_K$ (ours)	**74.9**	**69.1**	**99.4***	**65.7**	**88.4**		**85.6**	**83.9**	**74.7**	**99.4***	**93.0**

TABLE V: Quantitative comparisons between different combinations of methods on adversarially trained models (EAT). Inc-v3, Inc-v4, Res152, and IncRes are adopted as white-box models to generate untargeted adversarial examples, while EAT are used to test transferability of adversarial examples.

	Inc-v3			Inc-v4			Res152			IncRes		
Attacks	Inc-v3$_{ens3}$	Inc-v3$_{ens4}$	IncRes$_{ens}$	Inc-v3$_{ens3}$	Inc-v3$_{ens4}$	IncRes$_{ens}$	Inc-v3$_{ens3}$	Inc-v3$_{ens4}$	IncRes$_{ens}$	Inc-v3$_{ens3}$	Inc-v3$_{ens4}$	IncRes$_{ens}$
DTI-FGSM	23.2	25.6	14.2	17.1	20.4	11.1	33.8	33.9	24.1	25.2	25.4	20.8
DTI-FGNM$_N$ (ours)	34.3	36.2	22.7	26.4	28.8	18.4	45.5	44.4	36.2	36.3	35.5	32.4
DTI-FGNM$_K$ (ours)	**35.9**	**36.8**	**23.7**	**28.1**	**29.7**	**21.2**	**49.5**	**48.4**	**41.5**	**39.7**	**38.1**	**25.5**
DSI-FGSM	31.9	31.0	18.2	42.1	40.9	26.2	39.1	36.5	25.5	49.4	45.5	37.4
DSI-FGNM$_N$ (ours)	**55.5**	**55.9**	**36.9**	**64.2**	60.0	**47.0**	61.9	**58.5**	49.2	71.5	65.0	62.1
DSI-FGNM$_K$ (ours)	55.1	55.4	35.9	62.5	**60.3**	46.4	**64.4**	58.4	**50.3**	**71.6**	**65.4**	**62.2**
DTSI-FGSM	49.9	52.5	35.2	52.4	53.2	40.9	56.8	60.2	46.2	73.0	72.2	68.4
DTSI-FGNM$_N$ (ours)	60.3	62.2	**46.4**	58.9	59.7	51.8	64.1	66.7	57.2	76.7	74.7	74.5
DTSI-FGNM$_K$ (ours)	**60.7**	**62.9**	45.6	**62.5**	**64.3**	**53.3**	**68.3**	**68.4**	**60.2**	**80.6**	**78.1**	**76.9**
MDTSI-FGSM	**67.3**	69.2	**54.9**	**68.4**	69.4	57.8	67.5	70.4	62.1	78.8	79.4	77.5
MDTSI-FGNM$_N$ (ours)	66.7	69.5	53.5	67.6	68.5	58.9	67.4	70.2	61.4	**79.2**	80.8	78.3
MDTSI-FGNM$_K$ (ours)	67.2	**70.7**	54.5	**67.7**	**71.7**	**59.1**	**69.0**	**72.5**	**62.6**	78.8	**80.9**	**80.1**

of [3], *i.e.*, ensembling models by fusing their logit activations, here we present results of targeted attacks.

a) Attack against Normally Trained Models: In Table. VI, we present success rates of targeted attacks against NT. Adversarial examples are crafted on an ensemble of three models (ensemble model) using different methods, and transferred to remaining one model (hold-out model). Percentage of adversarial examples misclassified as target labels by ensemble and hold-out models represents success rate of targeted white-box and black-box attacks, respectively. As demonstrated in the table, attack performance of original methods can be improved in all cases by integrating our FGNM$_N$ and FGNM$_K$ with them. Under white-box setting, for example, our DI-FGNM$_N$, DI-FGNM$_K$ surpass DI-FGSM by **3.7%** and **6.8%** (on average), respectively. Under black-box setting, our methods can significantly enhance transferability of adversarial examples regardless of original FGSM-based methods or ensemble models. In particular, when using I-FGNM$_K$, DI-FGNM$_K$, TI-BNIM$_K$ and DTI-FGNM$_K$, to transfer to Inc-v3, targeted attack success rates have been increased by **9.3%**, **21.6%**, **11.6%**, and **23.1%** than vanilla methods. Intuitively, a possible reason is that bias of direction between gradients and perturbations caused by sign operations also affects results of targeted attack. Our FGNM$_K$ and FGNM$_N$ mitigate this bias and improve success rate of targeted attacks.

b) Attack against Defense Models: Applying targeted attacks on EAT is more difficult than NT. For the sake of comprehensiveness, we perform targeted attacks using different methods against EAT. Specifically, we firstly attack an ensemble of five models (three NT and two EAT). Then test targeted black-box, white-box attack results on remaining one EAT model (hold-out model) and ensemble model, respectively. Results are presented in Table. VII, it can be seen that targeted adversarial examples have worse transferability on EAT compared to NT (see Table. VI). DTI-FGSM, DTMI-FGSM, DTPoI-FGSM demonstrate their effectiveness due to use of diverse inputs, metric learning adopting Poincare distance, and translation-invariant attacks. However, the use of

TABLE VI: Success rates on normally trained models of targeted adversarial attacks compare to different methods against an ensemble of white-box models and a hold-out black-box target model. Where "-" indicates hold-out model. "*" denotes white-box results while others are black-box results.

Models	Attacks	-Inc-v3	-Inc-v4	-Res152	-IncRes
Ensemble	I-FGSM	99.9*	99.9*	**100.0***	**100.0***
	I-FGNM$_N$ (ours)	99.9*	99.9*	**100.0***	**100.0***
	I-FGNM$_K$ (ours)	**100.0***	**100.0***	**100.0***	**100.0***
	DI-FGSM	91.7*	91.3*	92.2*	93.7*
	DI-FGNM$_N$ (ours)	95.7*	96.0*	94.9*	97.2*
	DI-FGNM$_K$ (ours)	**99.1***	**99.1***	**98.5***	**99.3***
	TI-BIM	99.9*	99.9*	**100.0***	**100.0***
	TI-BNIM$_N$ (ours)	99.9*	99.9*	**100.0***	**100.0***
	TI-BNIM$_K$ (ours)	**100.0***	**100.0***	**100.0***	**100.0***
	DTI-FGSM	90.3*	89.7*	90.5*	94.4*
	DTI-FGNM$_N$ (ours)	95.3*	96.1*	95.6*	96.3*
	DTI-FGNM$_K$ (ours)	**98.2***	**99.0***	**98.1***	**99.4***
Hold-out	I-FGSM	1.2	0.6	0.0	0.4
	I-FGNM$_N$ (ours)	4.6	3.9	0.8	3.3
	I-FGNM$_K$ (ours)	**10.5**	**5.9**	**1.5**	**6.5**
	DI-FGSM	15.3	14.4	3.6	8.6
	DI-FGNM$_N$ (ours)	22.5	25.7	8.4	19.5
	DI-FGNM$_K$ (ours)	**36.9**	**36.2**	**13.1**	**32.1**
	TI-BIM	2.2	1.3	0.4	0.7
	TI-BNIM$_N$ (ours)	6.4	5.3	1.6	3.7
	TI-BNIM$_K$ (ours)	**13.8**	**10.7**	**3.8**	**8.6**
	DTI-FGSM	16.4	14.9	4.3	10.3
	DTI-FGNM$_N$ (ours)	26.4	26.8	9.3	21.9
	DTI-FGNM$_K$ (ours)	**39.5**	**41.0**	**13.7**	**35.8**

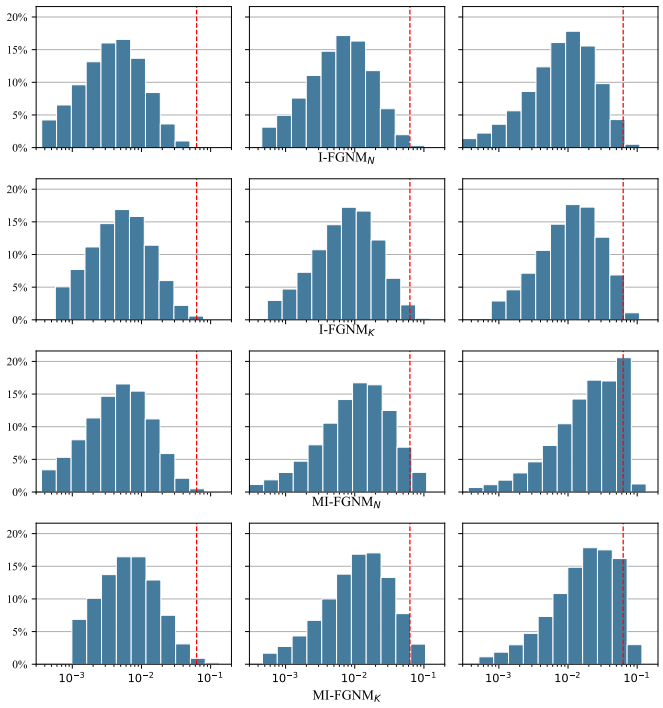


Fig. 7: Histogram of absolute perturbations before clipping at iteration 2, 5, 10 with I-FGNM$_N$, I-FGNM$_K$, MI-FGNM$_N$, and MI-FGNM$_K$, noises on the right side of the red dashed lines will be clipped. Compared to I-methods, MI-methods produces more perturbations to be clipped.

sign operation limits their attack performance. Our approach FGNM$_N$ and FGNM$_K$ mitigates side-effect of sign operation through adopting scale factor and further improves success rate of targeted attacks in most cases. Under white-box setting, our FGNM$_N$, FGNM$_K$ surpassing FGSM-based methods by **6.3%**, **12.7%** on average and **7.9%**, **15.1%** at most, respectively. Under black-box setting, it is **7.4%**, **8.3%** and **11.8%**, **18.5%**.

TABLE VII: Success rates on adversarially trained models of targeted adversarial attacks compare to different methods against an ensemble of white-box models and a hold-out black-box model. Where "-" indicates the hold-out network. "*" denotes the white-box results while others are black-box results.

Models	Attacks	Ensemble	Hold-out
-Inc-v3$_{ens3}$	DTI-FGSM	87.8*	3.6
	DTI-FGNM$_N$ (ours)	92.8*	15.4
	DTI-FGNM$_K$ (ours)	**98.5***	**22.1**
	DTMI-FGSM	83.4*	9.2
	DTMI-FGNM$_N$ (ours)	89.4*	15.1
	DTMI-FGNM$_K$ (ours)	**97.6***	**12.7**
	DTPoI-FGSM	83.1*	1.9
	DTPoI-FGNM$_N$ (ours)	91.0*	11.5
	DTPoI-FGNM$_K$ (ours)	**97.4***	**13.9**
-Inc-v3$_{ens4}$	DTI-FGSM	85.9*	3.0
	DTI-FGNM$_N$ (ours)	92.1*	14.8
	DTI-FGNM$_K$ (ours)	**98.3***	**19.6**
	DTMI-FGSM	93.2*	4.5
	DTMI-FGNM$_N$ (ours)	95.6*	**8.1**
	DTMI-FGNM$_K$ (ours)	**98.9***	4.8
	DTPoI-FGSM	82.5*	1.9
	DTPoI-FGNM$_N$ (ours)	89.8*	11.3
	DTPoI-FGNM$_K$ (ours)	**97.6***	**12.7**
-IncRes$_{ens}$	DTI-FGSM	86.3*	2.1
	DTI-FGNM$_N$ (ours)	93.4*	**9.6**
	DTI-FGNM$_K$ (ours)	**98.5***	**9.6**
	DTMI-FGSM	82.2*	**4.4**
	DTMI-FGNM$_N$ (ours)	89.9*	4.3
	DTMI-FGNM$_K$ (ours)	**96.8***	3.7
	DTPoI-FGSM	82.8*	0.7
	DTPoI-FGNM$_N$ (ours)	90.2*	7.4
	DTPoI-FGNM$_K$ (ours)	**97.7***	**6.9**

D. Analysis

1) Magnitude and precision of noise: For verifying that our method reduces side effects of sign operation, we report magnitude (ℓ_2-norm $\|\cdot\|$) and precision ($\cos\langle\cdot, \boldsymbol{g}\rangle$) of adversarial noises in Table. VIII. Given untargeted adversarial examples generated via NT using different methods, magnitude and precision of noises are averaged among the whole iteration. It can be observed that our FGNM$_N$ variants generate smaller and more accurate noises compared to original methods, *i.e.*, closer to gradient direction. For example, noises generated by I-FGNM$_N$, MI-FGNM$_N$ is on average **2.1%**, **11.2%** smaller than corresponding FGSM-based methods. It is worth noting that cos value of our fixed scale approach FGNM$_N$ does not reach 1.0 due to clip operation, but it is still higher than original methods I-FGSM, MI-FGSM by **0.4** and **0.2** (on average), respectively. Compared with FGNM$_N$, our FGNM$_K$ methods generate larger noise magnitudes and smaller cos values because of relaxed constraints on noise magnitudes. Nevertheless, cos value of FGNM$_K$ method is still higher than that of original FGSM-based method by **0.2** on average and **0.3** at most. Obviously, both FGNM$_N$ and FGNM$_K$ alleviate

TABLE VIII: Quantitative comparisons of average magnitude $\|\cdot\|$ and precision $\cos\langle\cdot, \boldsymbol{g}\rangle$ of noises. Given Inc-v3, Inc-v4, Res152 and IncRes as white-box models, adversarial examples are crafted by different methods including 1) FGSM-based, *e.g.*, IFGSM, *etc.*, 2) FGNM_N variants, *e.g.*, I-FGNM_N, *etc.*, 3) FGNM_K variants, *e.g.*, I-FGNM_K, *etc.*, where K is set to 12000.

Attacks	Inc-v3		Inc-v4		Res152		IncRes	
	$\|\cdot\|$	$\cos\langle\cdot, \boldsymbol{g}\rangle$	$\|\cdot\|$	$\cos\langle\cdot, \boldsymbol{g}\rangle$	$\|\cdot\|$	$\cos\langle\cdot, \boldsymbol{g}\rangle$	$\|\cdot\|$	$\cos\langle\cdot, \boldsymbol{g}\rangle$
I-FGSM	20.21	0.63	20.77	0.61	21.12	0.59	21.12	0.60
I-FGNM_N (ours)	**18.51**	**0.98**	**18.86**	**0.98**	**18.52**	**0.99**	**18.92**	**0.98**
I-FGNM_K (ours)	34.94	0.92	36.60	0.91	36.48	0.92	37.00	0.90
MI-FGSM	46.10	0.64	47.20	0.64	46.90	0.65	47.38	0.63
MI-FGNM_N (ours)	**35.91**	**0.82**	**36.11**	**0.81**	**35.17**	**0.83**	**35.69**	**0.80**
MI-FGNM_K (ours)	49.47	0.60	50.48	0.59	50.39	0.59	50.45	0.58
DI-FGSM	20.61	0.60	21.18	0.59	21.40	0.58	21.42	0.58
DI-FGNM_N (ours)	**18.76**	**0.98**	**19.03**	**0.97**	**18.86**	**0.99**	**18.98**	**0.97**
DI-FGNM_K (ours)	36.56	0.90	37.47	0.89	37.39	0.89	37.62	0.87
TI-BIM	21.33	0.67	21.89	0.64	23.06	0.61	23.07	0.63
TI-BNIM_N (ours)	**19.46**	**0.99**	**19.96**	**0.98**	**19.86**	**0.98**	**20.23**	**0.98**
TI-BNIM_K (ours)	34.61	0.94	35.99	0.93	36.85	0.90	36.70	0.91
SI-FGSM	22.48	0.65	23.00	0.64	22.80	0.57	23.46	0.62
SI-FGNM_N (ours)	**19.99**	**0.99**	**20.15**	**0.99**	**19.57**	**0.97**	**20.25**	**0.98**
SI-FGNM_K (ours)	35.68	0.92	36.57	0.93	36.55	0.91	37.01	0.89
DTI-FGSM	21.62	0.65	21.89	0.64	22.75	0.62	23.06	0.63
DTI-FGNM_N (ours)	**19.90**	**0.98**	**19.96**	**0.98**	**20.39**	**0.98**	**20.22**	**0.98**
DTI-FGNM_K (ours)	35.65	0.93	36.99	0.93	37.67	0.90	36.72	0.91
DSI-FGSM	23.10	0.64	23.57	0.63	23.44	0.62	24.03	0.59
DSI-FGNM_N (ours)	**20.55**	**0.98**	**20.52**	**0.98**	**20.27**	**0.97**	**20.62**	**0.97**
DSI-FGNM_K (ours)	36.17	0.92	36.90	0.89	36.79	0.86	37.33	0.88
DTSI-FGSM	25.71	0.67	26.00	0.64	26.60	0.66	28.19	0.62
DTSI-FGNM_N (ours)	**23.23**	**0.98**	**22.99**	**0.97**	**23.42**	**0.97**	**24.16**	**0.96**
DTSI-FGNM_K (ours)	37.09	0.92	37.61	0.90	38.38	0.85	38.74	0.87
MDTSI-FGSM	41.48	0.67	41.71	0.62	42.25	0.66	43.87	0.62
MDTSI-FGNM_N (ours)	**34.67**	**0.88**	**34.25**	**0.85**	**34.22**	**0.86**	**33.93**	**0.82**
MDTSI-FGNM_K (ours)	47.56	0.71	47.75	0.67	48.03	0.67	48.21	0.62

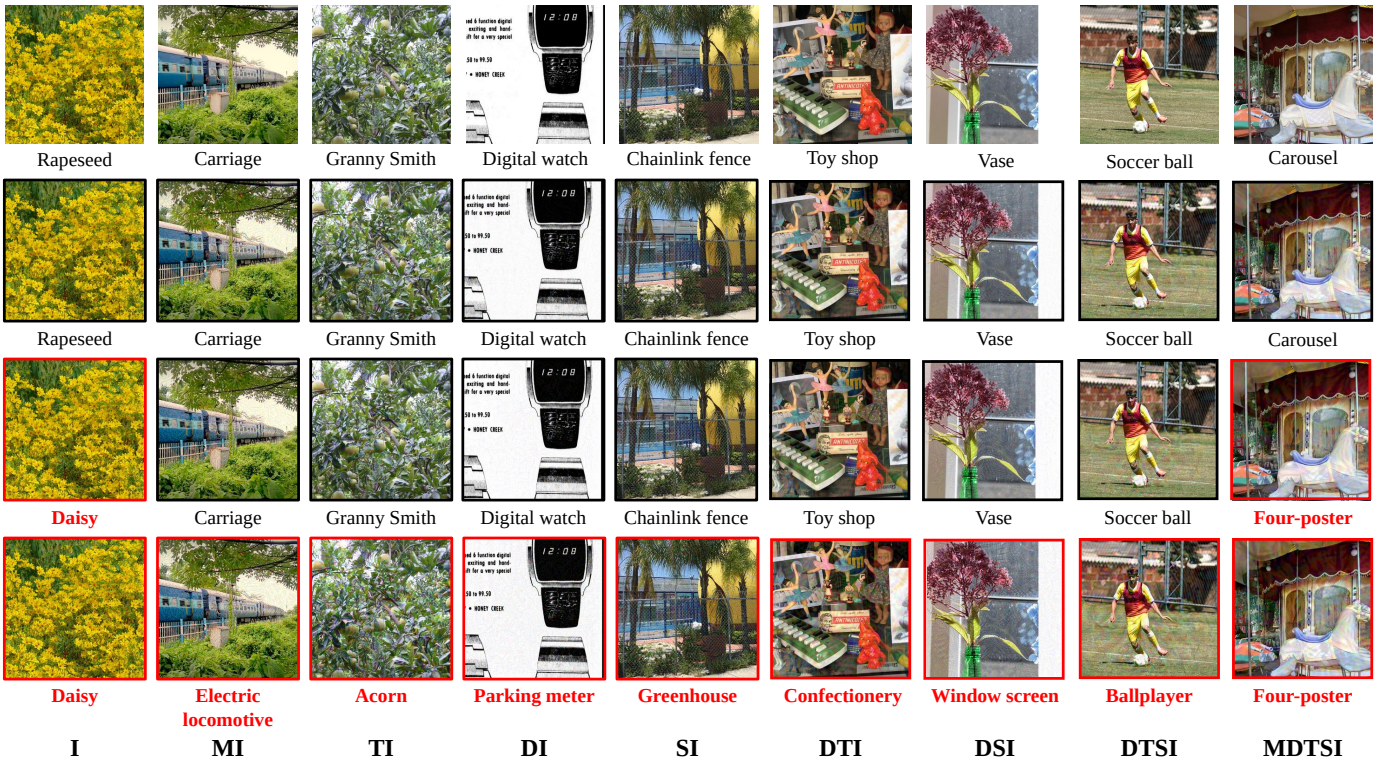


Fig. 8: Visualization of adversarial examples. From top to bottom row-by-row: 1) raw images, 2) methods using sign operation, 3) methods with our fixed scale, *e.g.*, I-FGNM_N *etc.*, and 4) methods with our adaptive scale, *e.g.*, TI-BNIM_K *etc.*, where K is set to $12,000$. From left to right are the basic algorithms adopted. We choose images generated by Inc-v3 white-box and tested them on Inc-v4. The predictions are placed below the images, and misclassified are highlighted in red.

side effects of sign operation and reduce gaps between real gradients and actual noises.

2) Analysis of MI-FGNM: Experimental results show that the performance gain on MI-FGNM$_{\mathrm{N}}$ is not significant compared with other methods. A potential reason is that MI-FGSM applies momentum term to the perturbations generation. The accumulated noises lead to a larger clipped ratio than other methods and hinder the performance of MI-FGNM$_{\mathrm{N}}$. Further experiments are conducted to verify this. Given Inc-v3 as the white-box model, we report the magnitude of noises before clipping over the whole dataset at iteration 2, 5, and 10 using various methods, including I-FGNM$_{\mathrm{N}}$, I-FGNM$_{\mathrm{K}}$, MI-FGNM$_{\mathrm{N}}$, MI-FGNM$_{\mathrm{K}}$. As demonstrated in Figure 7, the clipped ratio of I-FGNM$_{\mathrm{N}}$ at iteration 2, 5, and 10 is 0.07%, 0.03% and 0.8% respectively. For I-FGNM$_{\mathrm{K}}$, it is 0.2%, 0.8%, and 1.5%. For MI-FGNM$_{\mathrm{N}}$, it is 0.2%, 3.7%, 15%. For MI-FGNM$_{\mathrm{K}}$, it is 0.6%, 3.5%, 7.6%. In brief, no more than 0.8% of perturbations in I-FGNM$_{\mathrm{N}}$ will be clipped, but for MI-FGNM$_{\mathrm{N}}$, the percentage increases to 15.0%. The larger clipped ratio distorts the direction of perturbations and decreases the magnitude of the final noise, which further hinders performance of MI-FGNM$_{\mathrm{N}}$. Unlike MI-FGNM$_{\mathrm{N}}$, MI-FGNM$_{\mathrm{K}}$ considers the trade-off between magnitude and bias to increase performance.

3) Visualization: Visualizations of adversarial examples are given to give qualitative analysis and confirm the effectiveness of generated perturbations. Specifically, we randomly choose several successful adversarial images for each approach, *i.e.*, I-FGSM, MI-FGSM, DI-FGSM, TI-BIM, SI-FGSM, DTI-FGSM, DSI-FGSM, DTSI-FGSM, and MDTSI-FGSM and plot the results in Figure 8. In this figure, the first row is the raw image while the remaining rows are adversarial examples crafted by original methods and ours FGNM$_{\mathrm{N}}$ and FGNM$_{\mathrm{K}}$ variants, respectively. As shown in the figure, noises are difficult to distinguish between original methods and ours visually. Notably, our FGNM$_{\mathrm{N}}$ variants produce nearly the same adversarial examples with originals, and FGNM$_{\mathrm{K}}$ variant slightly increases the noise level. The visualization indicates that our methods can easily boost performance without adding significant noises.

V. Conclusion

Based on the Taylor expansion, we conduct a comprehensive analysis of gradient-based methods' sign operation and reveal the gap between real gradients and resultant noises, leading to biased and inefficient attacks. A novel routine named Fast Gradient Non-sign Methods is proposed to correct this gap. Notably, FGNM is a general routine that seamlessly replaces the conventional $sign$ operation in gradient-based attacks with negligible extra computational cost. To confirm the effectiveness of our FGNM, extensive experiments under non-targeted and targeted ℓ_∞ settings are conducted. Significant performance gains are observed compared with state-of-the-art methods. For untargeted black-box attacks, ours outperform them by **27.5%** at most and **9.5%** on average. For targeted attacks against defense models, it is **15.1%** and **12.7%**.

References

[1] I. J. Goodfellow, J. Shlens, and C. Szegedy, "Explaining and harnessing adversarial examples," in *ICLR*, 2015.

[2] A. Kurakin, I. J. Goodfellow, and S. Bengio, "Adversarial examples in the physical world," in *ICLR*, 2017.

[3] Y. Dong, F. Liao, T. Pang, H. Su, J. Zhu, X. Hu, and J. Li, "Boosting adversarial attacks with momentum," in *CVPR*, 2018.

[4] C. Xie, Z. Zhang, Y. Zhou, S. Bai, J. Wang, Z. Ren, and A. L. Yuille, "Improving transferability of adversarial examples with input diversity," in *CVPR*, 2019.

[5] Y. Dong, T. Pang, H. Su, and J. Zhu, "Evading defenses to transferable adversarial examples by translation-invariant attacks," in *CVPR*, 2019.

[6] L. Gao, Q. Zhang, J. Song, X. Liu, and H. T. Shen, "Patch-wise attack for fooling deep neural network," in *ECCV*, 2020.

[7] M. Li, C. Deng, T. Li, J. Yan, X. Gao, and H. Huang, "Towards transferable targeted attack," in *CVPR*, 2020.

[8] M. Yin, Y. Zhang, X. Li, and S. Wang, "When deep fool meets deep prior: Adversarial attack on super-resolution network," in *MM*, 2018.

[9] M. Li, C. Deng, T. Li, J. Yan, X. Gao, and H. Huang, "Towards transferable targeted attack," in *CVPR*, 2020.

[10] X. Dong, J. Han, D. Chen, J. Liu, H. Bian, Z. Ma, H. Li, X. Wang, W. Zhang, and N. Yu, "Robust superpixel-guided attentional adversarial attack," in *CVPR*, 2020.

[11] W. Wu, Y. Su, X. Chen, S. Zhao, I. King, M. R. Lyu, and Y. Tai, "Boosting the transferability of adversarial samples via attention," in *CVPR*, 2020.

[12] A. Liu, J. Wang, X. Liu, B. Cao, C. Zhang, and H. Yu, "Bias-based universal adversarial patch attack for automatic check-out," in *ECCV*, 2020.

[13] K. Eykholt, I. Evtimov, E. Fernandes, B. Li, A. Rahmati, C. Xiao, A. Prakash, T. Kohno, and D. Song, "Robust physical-world attacks on deep learning visual classification," in *CVPR*, 2018.

[14] M. Sharif, S. Bhagavatula, L. Bauer, and M. K. Reiter, "Accessorize to a crime: Real and stealthy attacks on state-of-the-art face recognition," in *CCS*, 2016.

[15] B. Yan, D. Wang, H. Lu, and X. Yang, "Cooling-shrinking attack: Blinding the tracker with imperceptible noises," in *CVPR*, 2020.

[16] Y. Lu, Y. Jia, J. Wang, B. Li, W. Chai, L. Carin, and S. Velipasalar, "Enhancing cross-task black-box transferability of adversarial examples with dispersion reduction," in *CVPR*, 2020.

[17] Z. Kong, J. Guo, A. Li, and C. Liu, "Physgan: Generating physical-world-resilient adversarial examples for autonomous driving," in *CVPR*, 2020.

[18] Z. Che, A. Borji, G. Zhai, S. Ling, J. Li, Y. Tian, G. Guo, and P. L. Callet, "Adversarial attack against deep saliency models powered by non-redundant priors," *IEEE Trans. Image Process.*, vol. 30, pp. 1973–1988, 2021.

[19] S. Moosavi-Dezfooli, A. Fawzi, and P. Frossard, "Deepfool: A simple and accurate method to fool deep neural networks," in *CVPR*, 2016.

[20] N. Carlini and D. A. Wagner, "Towards evaluating the robustness of neural networks," in *SP*, 2017.

[21] W. Brendel, J. Rauber, and M. Bethge, "Decision-based adversarial attacks: Reliable attacks against black-box machine learning models," in *ICLR*, 2018.

[22] N. Papernot, P. D. McDaniel, I. J. Goodfellow, S. Jha, Z. B. Celik, and A. Swami, "Practical black-box attacks against machine learning," in *AsiaCCS*, 2017.

[23] Y. Liu, X. Chen, C. Liu, and D. Song, "Delving into transferable adversarial examples and black-box attacks," in *ICLR*, 2017.

[24] J. Lin, C. Song, K. He, L. Wang, and J. E. Hopcroft, "Nesterov accelerated gradient and scale invariance for adversarial attacks," 2020.

[25] L. Gao, Y. Cheng, Q. Zhang, X. Xu, and J. Song, "Feature space targeted attacks by statistic alignment," in *IJCAI*.

[26] Y. Zhang, X. Tian, Y. Li, X. Wang, and D. Tao, "Principal component adversarial example," *IEEE Trans. Image Process.*, vol. 29, pp. 4804–4815, 2020.

[27] J. Wang, A. Liu, X. Bai, and X. Liu, "Universal adversarial patch attack for automatic checkout using perceptual and attentional bias," *IEEE Trans. Image Process.*, vol. 31, pp. 598–611, 2022.

[28] J. Chen, M. I. Jordan, and M. J. Wainwright, "Hopskipjumpattack: A query-efficient decision-based attack," in *SP*, 2020.

[29] M. Sharif, S. Bhagavatula, L. Bauer, and M. K. Reiter, "Accessorize to a crime: Real and stealthy attacks on state-of-the-art face recognition," in *CCS*, 2016.

[30] D. Kumar, C. Kumar, C. Seah, S. Xia, and M. Shao, "Finding achilles' heel: Adversarial attack on multi-modal action recognition," in *MM*, 2020.
[31] R. Wang, F. Juefei-Xu, Q. Guo, Y. Huang, X. Xie, L. Ma, and Y. Liu, "Amora: Black-box adversarial morphing attack," in *MM*, 2020.
[32] J. Ji, X. Sun, Y. Zhou, R. Ji, F. Chen, J. Liu, and Q. Tian, "Attacking image captioning towards accuracy-preserving target words removal," in *MM*, 2020.
[33] C. Ma, W. Meng, B. Wu, S. Xu, and X. Zhang, "Efficient joint gradient based attack against SOR defense for 3d point cloud classification," in *MM*, 2020.
[34] G. S. Dhillon, K. Azizzadenesheli, Z. C. Lipton, J. Bernstein, J. Kossaifi, A. Khanna, and A. Anandkumar, "Stochastic activation pruning for robust adversarial defense," in *ICLR*, 2018.
[35] N. Liu, H. Yang, and X. Hu, "Adversarial detection with model interpretation," in *SIGKDD*, 2018.
[36] X. Liu, Y. Li, C. Wu, and C. Hsieh, "Adv-bnn: Improved adversarial defense through robust bayesian neural network," in *ICLR*, 2019.
[37] J. H. Metzen, T. Genewein, V. Fischer, and B. Bischoff, "On detecting adversarial perturbations," in *ICLR*, 2017.
[38] C. Guo, M. Rana, M. Cissé, and L. van der Maaten, "Countering adversarial images using input transformations," in *ICLR*, 2018.
[39] C. Xie, J. Wang, Z. Zhang, Z. Ren, and A. L. Yuille, "Mitigating adversarial effects through randomization," in *ICLR*, 2018.
[40] A. Mustafa, S. H. Khan, M. Hayat, J. Shen, and L. Shao, "Image super-resolution as a defense against adversarial attacks," *IEEE Trans. Image Process.*, vol. 29, pp. 1711–1724, 2020.
[41] S. Gu and L. Rigazio, "Towards deep neural network architectures robust to adversarial examples," in *ICLR*, 2015.
[42] Z. Zhao, H. Wang, H. Sun, J. Yuan, Z. Huang, and Z. He, "Removing adversarial noise via low-rank completion of high-sensitivity points," *IEEE Trans. Image Process.*, vol. 30, pp. 6485–6497, 2021.
[43] X. Zhang, J. Wang, T. Wang, R. Jiang, J. Xu, and L. Zhao, "Robust feature learning for adversarial defense via hierarchical feature alignment," *Inf. Sci.*, vol. 560, pp. 256–270, 2021.
[44] F. Tramèr, A. Kurakin, N. Papernot, I. J. Goodfellow, D. Boneh, and P. D. McDaniel, "Ensemble adversarial training: Attacks and defenses," in *ICLR*, 2018.
[45] A. Madry, A. Makelov, L. Schmidt, D. Tsipras, and A. Vladu, "Towards deep learning models resistant to adversarial attacks," in *ICLR*, 2018.
[46] C. Szegedy, V. Vanhoucke, S. Ioffe, J. Shlens, and Z. Wojna, "Rethinking the inception architecture for computer vision," in *CVPR*, 2016.
[47] C. Szegedy, S. Ioffe, V. Vanhoucke, and A. Alemi, "Inception-v4, inception-resnet and the impact of residual connections on learning," in *AAAI*, 2017.
[48] K. He, X. Zhang, S. Ren, and J. Sun, "Deep residual learning for image recognition," in *CVPR*, 2016.
[49] C. Szegedy, S. Ioffe, V. Vanhoucke, and A. Alemi, "Inception-v4, inception-resnet and the impact of residual connections on learning," in *AAAI*, 2017.
[50] G. Huang, Z. Liu, L. Van Der Maaten, and K. Q. Weinberger, "Densely connected convolutional networks," in *CVPR*, 2017.